Mechanical Systems and Signal Processing 193 (2023) 110256

Contents lists available at ScienceDirect

Mechanical Systems and Signal Processing

journal homepage: www.elsevier.com/locate/ymssp

Parametric excitation as a cause of clutch judder: theoretical study and experimental validation

Manuel Tentarelli [a,*], Stefano Cantelli [b], Silvio Sorrentino [a], Alessandro De Felice [a]

[a] University of Modena and Reggio Emilia, Department of Engineering 'Enzo Ferrari', Via Vivarelli 10, Modena 41125, Italy
[b] CNH Industrial Italia, Via delle Nazioni 55, Modena 41122, Italy

ARTICLE INFO

Keywords:
Automotive driveline
Clutch judder
Parametric excitation
Stability map
Floquet analysis

ABSTRACT

Judder is a friction-induced torsional vibration generated during clutch engagement in automotive drivelines. To the best of the authors' knowledge, three are the causes attributed by the scientific community to the onset of the clutch judder: stick-slip phenomena, negative gradient of the coefficient of friction and geometric disturbances.

With the help of a methodological approach that integrates the analysis of a mathematical model with the experimental data obtained on a specially designed test bench, this paper shows that, in some cases, the clutch judder may also be due to the presence of parametric excitation.

This new understanding overcomes the limits of the existing explanations because it does not preclude the occurrence of clutch judder at high slip speeds, with positive gradients of the friction coefficient and at excitation frequencies different from the eigenfrequencies of the system.

The four degrees of freedom model developed for the study of the transmission provides maps that allow to identify the instability conditions of the system. The analysis described in this paper has been aimed at solving a judder problem in a transmission already in production, but the same approach can be used to avoid the conditions that cause the onset of clutch judder on other transmissions in the design phase.

1. Introduction

Nowadays, both the manufacturer and the consumer consider ride comfort an essential aspect of a vehicle's performance. Among several sources of discomfort, problems related to noise and vibrations induced by the driveline occupy a prominent place. In particular, the so-called clutch judder plays an important role since it can manifest itself as both noise and vibration transmitted to the driver.

Although clutch judder is commonly identified by a vibration with frequencies between 5 and 20 Hz [1], several studies have investigated the phenomenon in a frequency range between 200 and 1000 Hz [2], including the analysis of 'eek' and 'squeal' noise in dry automotive clutches [3,4], as well as wobbling instability in friction discs [5]. In this second frequency range clutch judder is mainly perceived as a noise and takes the name of 'squawk', 'squeal' or 'eek' depending on the frequency at which it occurs. Further studies [6] have investigated other frequency ranges at which judder can occur by including the influence of the clutch surface temperature and have shown that the spectrum of the vibration can change according to the temperature level.

The scientific community commonly classifies the clutch judder into Self-Induced Judder (SIJ) and Pressure-Induced Judder (PIJ).

* Corresponding author.
E-mail address: manuel.tentarelli@unimore.it (M. Tentarelli).

https://doi.org/10.1016/j.ymssp.2023.110256
Received 3 October 2022; Received in revised form 1 January 2023; Accepted 27 February 2023
Available online 5 March 2023

Nomenclature

J_1	Moment of inertia of body on the engine side
J_2	Moment of inertia of clutch damper
J_3	Moment of inertia of body on the gearbox side
J_4	Moment of inertia of body between clutch damper and clutch discs
θ_1	Angular displacement of body on the engine side
θ_2	Angular displacement the clutch damper
θ_3	Angular displacement of body on the gearbox side
θ_4	Angular displacement of body between clutch damper and clutch discs
t	Time
k_{ij}	Torsional stiffnesses
c_i	External damping coefficients
c_{ij}	Internal damping coefficients
ζ_{ij}	Damping factor related to coefficient c_{ij}, to k_{ij} and to J_j
T_e	Engine torque
T_c	Friction torque
T_r	Resistant torque
N_c	Number of pairs of clutch plates
R_m	Mean radius of the clutch friction surfaces
S	Area of action of the clutch actuation pressure
μ_0	Clutch friction coefficient, constant component with respect to time
μ_g	Clutch friction coefficient, gradient with respect to relative angular velocity
p_m	Amplitude of the constant component of the clutch actuation pressure
p_f	Amplitude of the fluctuating component of the clutch actuation pressure
ω_p	Angular frequency of the fluctuating component of the clutch actuation pressure

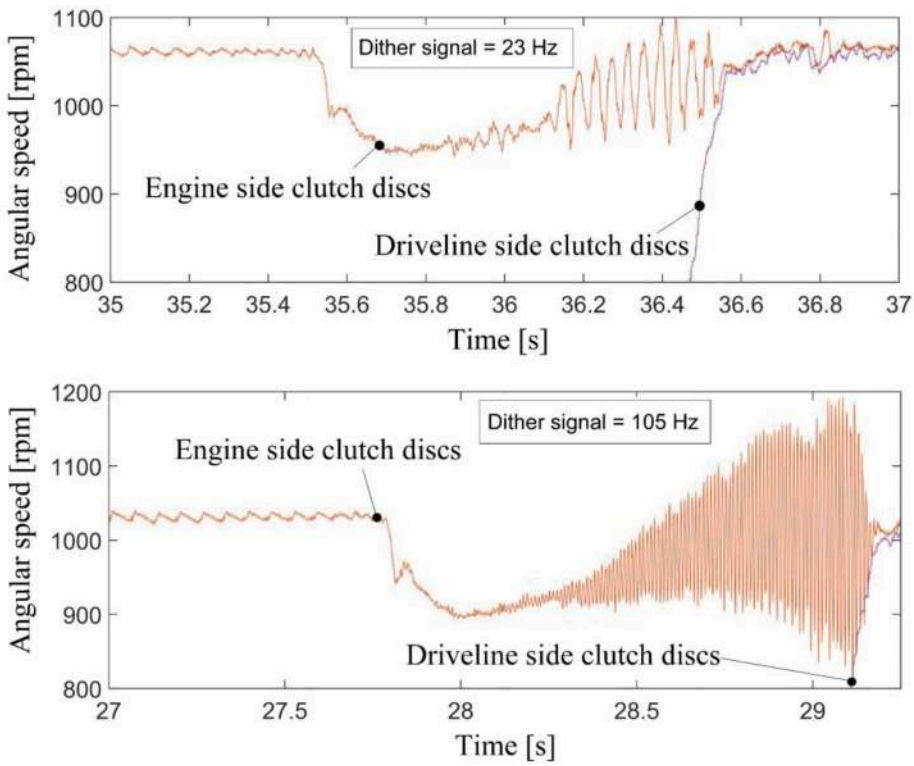

Fig. 1. Time histories for two engagements with judder, with different dither frequencies (23 Hz and 105 Hz). In both cases, judder occurs at the same frequency as dither.

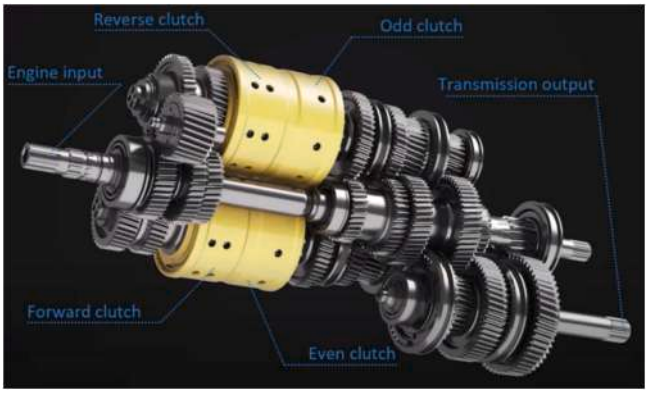

Fig. 2. The 24×24 Dynamic Command transmission (source: CNH Industrial).

Several researchers have associated the SIJ with a negative gradient of the friction coefficient with respect to the slip speed [1,7]. This basic mechanism can explain the onset of self-excited vibrations during engagements of dry friction clutches [8,9], wet friction clutches [10], in both manual [11] and automatic transmissions [12], as well as in dual clutch transmissions [13]. This analysis was also extended to consider nonlinear effects [14,15]. However, in [16] it was concluded that a negative value of the gradient of the friction coefficient is a sufficient condition only for causing judder. Other studies have correlated SIJ to the stick-slip phenomenon [6,14], with reference to dry friction contacts [17], frequency locking phenomena [18], and clutch ageing [19]. Nevertheless, this explanation cannot justify the cases when judder occurs at the beginning of the clutch engagement, because stick-slip only occurs at near-zero slip speeds.

On the other hand, the PIJ can have two trigger mechanisms. Firstly, the presence of hot spots due to the inevitable irregularities of the sliding surfaces of the plates can induce thermoelastic instability [20,21]. Secondly, misalignments of the transmission components can lead to cyclic variations of the clamp load and consequently to torque fluctuations [14,22]. When the angular velocity of the clutch discs equals a frequency of vibration of the driveline, a resonance occurs, and torsional oscillations are amplified [23].

The anomalous vibration investigated in the present study occurs on the CNH tractor dual-clutch transmission called 24×24 Dynamic Command transmission, equipped with wet clutches and electro-hydraulic actuation (transmission specifications in Section 2.1). This phenomenon is not comparable to any of the types of clutch judder cited in the specialist literature. It manifests itself during slip operation mode as both vibration and ‘squawk’ noise and has the same frequency as the oscillating component of the actuation pressure signal (called dither).

The clutches, in which the judder has occurred, are implemented by fluctuating the oil pressure to improve valve response [24] and reduce the control errors due to stiction and hysteresis. The fluctuation is obtained by applying a sinusoidal signal (dither) to the solenoid current. Although some studies have shown that oil pressure fluctuation can worsen stick-slip [25] or, in some cases, it can amplify clutch judder if its frequency equals a vibration frequency of the system [23], the mechanisms of onset of the phenomenon remain the same and are not enough to explain the ‘squawk’ noise observed. In fact, negative gradients of the friction coefficient or geometric disturbances would produce unstable oscillations at a frequency depending on the system parameters only, while stick-slip would occur at small relative angular speeds of the discs. On the contrary, the vibration examined in this paper occurs at the dither frequency and at high slip speeds. Fig. 1 shows two different time histories for engagements with judder, with different dither frequencies (23 Hz and 105 Hz): in both cases, judder occurs at the same frequency as dither, on the engine side clutch discs and at high relative angular speed between discs.

Therefore, in their previous work [26], the authors of this study proposed a minimal model of the transmission, able to explain the occurrence of judder as a parametrically excited vibration due to hydraulic actuation of the clutch.

In the present research, developed in partnership with CNH Industrial Italia, this kind of judder is investigated by processing experimental data (time histories) acquired on a specifically designed test bench [27]. The processed data are collected in diagrams drawn as functions of the two excitation parameters, i.e., frequency and amplitude of dither, at different values of lubricating oil temperature and engine angular speed.

A minimal model with 4 degrees of freedom (dofs) is then proposed. This model is able to fit the experimental data and to explain the onset of the parametrically excited vibration by identifying which parameters have a major role in controlling the phenomenon. In this way, it is possible to draw maps that allow to predict instability conditions and to avoid them already in the design phase.

2. Dual clutch transmission and test bench

2.1. Description of the dual clutch transmission under analysis

The transmission under study is called 24×24 Dynamic Command transmission, it is equipped with four multi-plate wet clutches with electro-hydraulic actuation and offers 24 different forward speed ratios due to the combination of eight ratios and three speed ranges. Compared to classic dual-clutch architectures, this transmission is equipped with two additional clutches that reverse the

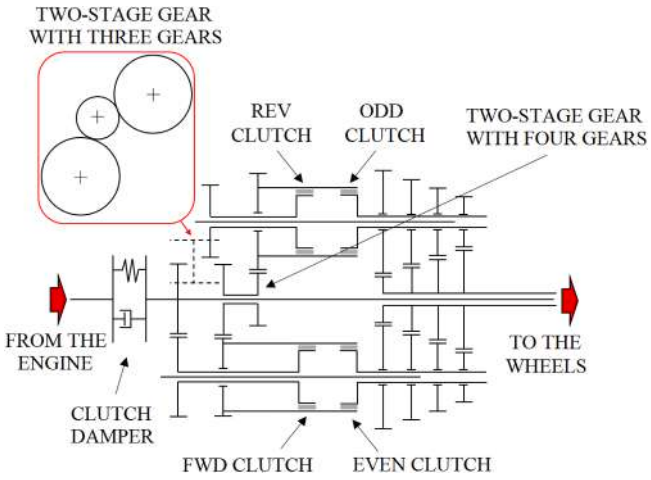

Fig. 3. Schematic of the 24×24 Dynamic Command transmission.

Fig. 4. Test bench.

direction of travel (Fig. 2).

The ODD and EVEN clutches manage the gear change and engage the odd and even gears respectively, according to the logic of standard dual clutches. On the other hand, the FWD and REV clutches are used to reverse the direction of travel and have a couple of discs more than the ODD and EVEN because they must stand higher torques during the engagement. A torsional damper is placed between the engine output and the clutch housings.

The FWD-EVEN and REV-ODD clutch pairs are coupled in twin housings. The even and odd gears downstream of the clutches are identical as well. The different speed ratio between even and odd gears is obtained by a two-stage gear with four gears placed upstream of the clutches. On the other hand, the reversal of the direction of travel is obtained by a two-stage gear with three gears upstream of the REV clutch (Fig. 3).

A vibration is superimposed on the opening and closing movement of the hydraulic valves that control the actuation of the clutches. This expedient is implemented by energizing the valve solenoid with a square wave signal, called dither, and has the purpose of reducing control errors due to stiction and hysteresis. In this way, the pressure signal that engages the clutches consists of two components: a constant component, plus a small amplitude oscillating term.

2.2. Description of the test bench

To reproduce the judder occurring in the transmission, and to study the effects of those parameters characterizing different operational conditions on its onset and development, a test bench was set up using a slightly modified gearbox (Fig. 4). These modifications were introduced to reproduce the real operating conditions, while allowing simplified test procedures. The test bench allowed to standardize the tests, focusing on the behaviour of the clutches.

The gearbox was modified as follows:

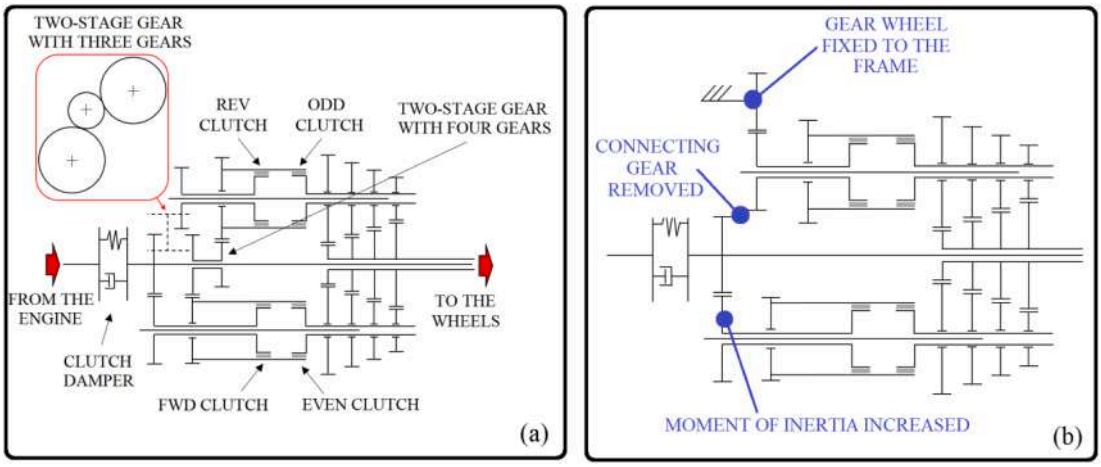

Fig. 5. Schematic of: original transmission (a) and modified transmission on the test bench (b).

- the connection between the shafts of the even and odd gears was removed;
- the gear wheel connected to the REV clutch was decoupled from the input shaft and fixed to the frame;
- the moment of inertia between damper and clutch pack was increased.

The first modification allows to always keep both the FWD and ODD clutches engaged, and to study the engagement by operating only the EVEN clutch. The second modification makes it possible to use the REV clutch as a resistant load. The third modification allows to consider the inertia of the removed connection to the ODD shaft.

The test bench is driven by an 81 kW DC electric motor. At low speed this engine delivers 680 Nm, which is enough to simulate a gear change. A schematic of the modified transmission is shown in Fig. 5.

The tests were carried out with the following input parameters:

- the angular speed of the electric motor which simulates the engine of the tractor;
- the main actuation pressure, the dither (fluctuating) pressure and the dither frequency for each of the four clutches.

The main and fluctuating components of the actuation pressure of the clutches were set on the test bench in terms of the current intensity that drives the control solenoid valve.

The quantities acquired during the tests were:

- the angular speed of the clutch plates on the engine side;
- the angular speed of the clutch plates on the gearbox side;
- the temperature of the lubricating oil near the EVEN clutch;
- the gearbox oil temperature;
- the pressures on the lines of actuation of all clutches.

The tests were carried out by operating only the EVEN clutch and keeping the FWD, ODD and REV clutches engaged. The main actuation pressures were kept constant at the following values of current intensity:

- 1000 mA for the FWD and ODD, corresponding to a pressure of about 21.5 bar (2.15 MPa);
- 670 mA for the REV, corresponding to a pressure of about 9.8 bar (0.98 MPa);
- 685 mA for the EVEN, corresponding to a pressure of about 10 bar (1 MPa).

With this setting, the FWD and ODD clutches do not slip, while the REV clutch slips, acting as a resistant load when the EVEN clutch is engaged.

The most important parameters for the identification of the clutch judder are certainly the angular speeds of the transmission shafts. The angular speeds were measured with two magnetic pick-ups: one installed upstream of the clutch housing, the other positioned downstream.

The sampling rates of magnetic pick-ups depend on the number of teeth of the gear wheel. In particular, the pick-up upstream of the clutches detects the speed of a wheel with 41 teeth, therefore at 1000 rpm it is capable of 684 acquisitions per second. This sampling rate is sufficient to cover the frequency range of interest for the experimental investigation.

As for the hydraulic circuit, the test bench is equipped with a high-pressure line, for the engagement of the clutches, and a low-pressure line, for lubrication and cooling (Fig. 6a).

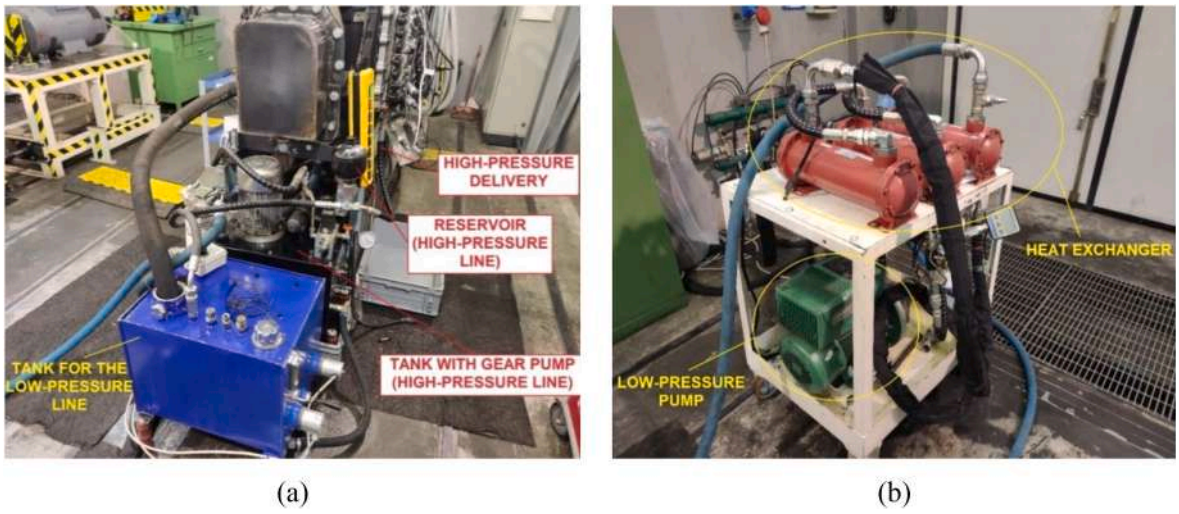

Fig. 6. Test bench hydraulic circuit. (a) High- and low-pressure lines and (b) heat exchanger.

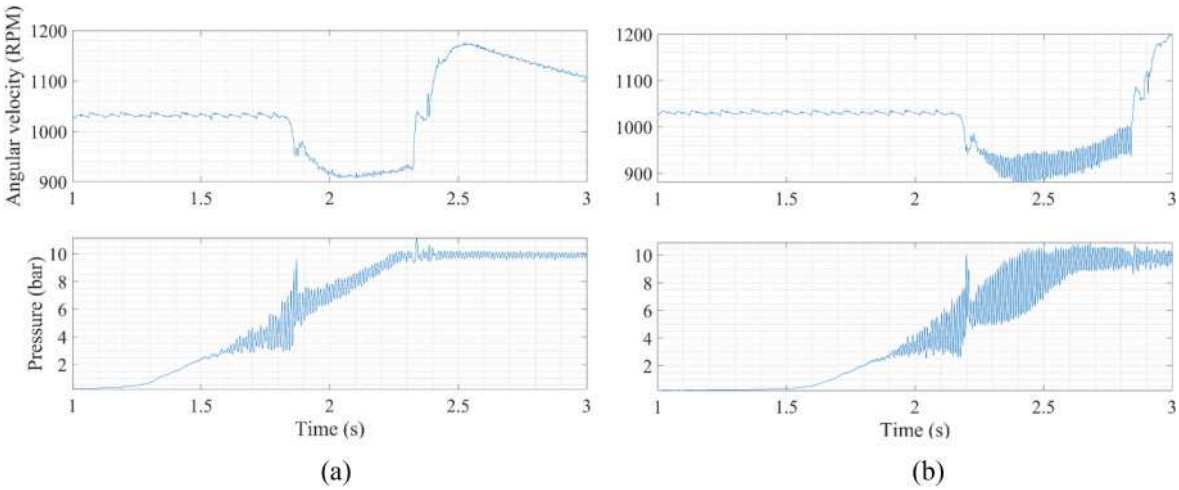

Fig. 7. Comparison between a correct engagement (a) and an engagement with instability (b).

The low-pressure line includes a water heat exchanger, aimed at keeping the oil temperature as constant as possible during the tests (Fig. 6b).

3. Experimental data

3.1. Measured signals

An experimental campaign was carried out to identify the operating conditions that cause an anomalous growth of torsional oscillations in the driveline. The two operating parameters that were varied during the tests are the frequency and the amplitude of the dither signal, yielding a frequency ω_p and an amplitude p_f of vibration of the actuation pressure. All tests were carried out by keeping as constant as possible the temperature near the actuated clutch (EVEN) as well as the temperature in the gearbox.

The angular speed upstream of the EVEN clutch was found to be the most sensitive quantity to the observed phenomenon, therefore it was taken as an indicator for the onset of the clutch judder (Fig. 7).

When judder occurs, the time histories of the angular speed upstream of the clutch show an anomalous vibration that arises at the beginning of the engagement (Fig. 7b), which excludes the hypothesis of stick-slip as the cause of the phenomenon.

Furthermore, Fourier analysis of the pressure and angular speed signals confirm that the frequency of the observed judder is always coincident with the frequency of dither, in all the different operating conditions that were tested, as those reported as an example in Fig. 8. This second evidence also excludes the classical case of direct excitation of an eigenmode of the transmission, possibly leading to

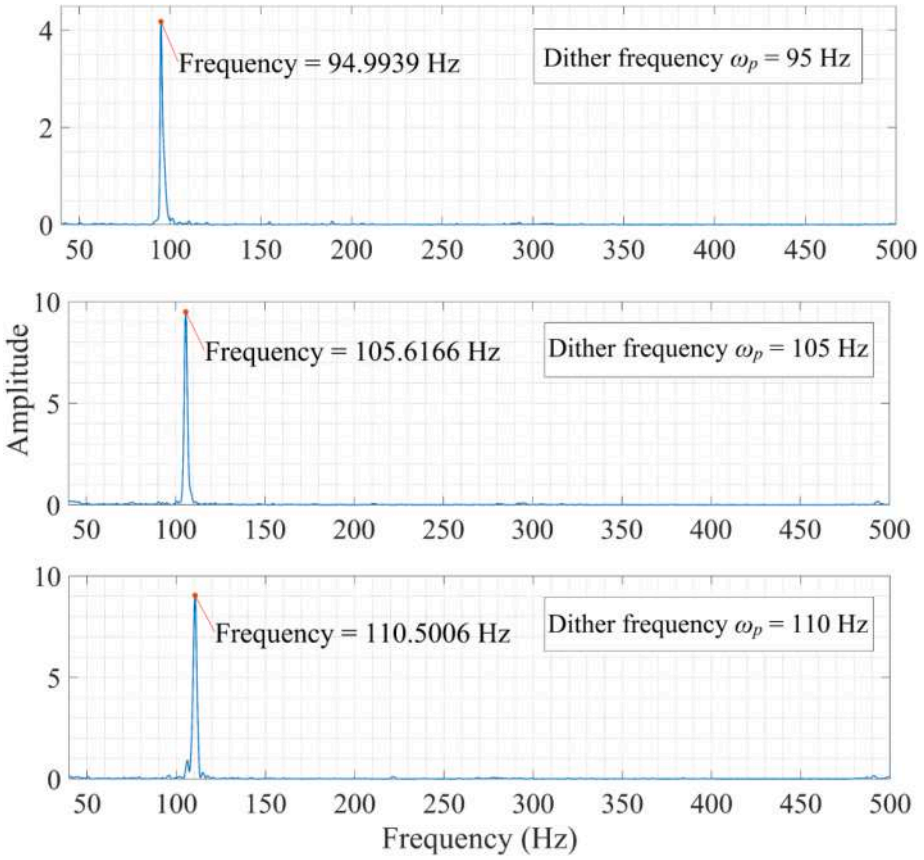

Fig. 8. Judder frequency coincides with dither frequency and varies with it.

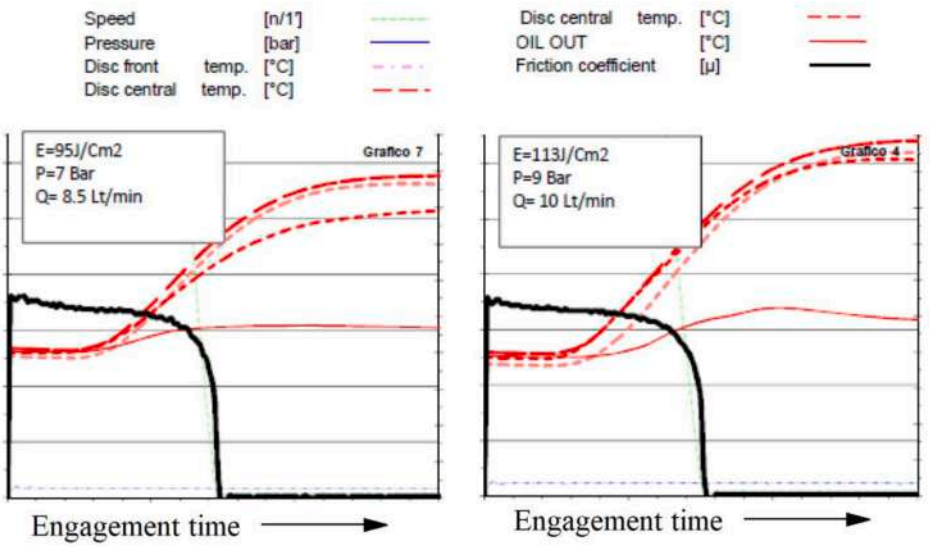

Fig. 9. Experimental graphs of the friction coefficient for the clutch under analysis. The reduction in the friction coefficient during clutch engagement is equivalent to a positive gradient in the friction coefficient with respect to the slip speed (the values on the axes have been deleted for confidentiality).

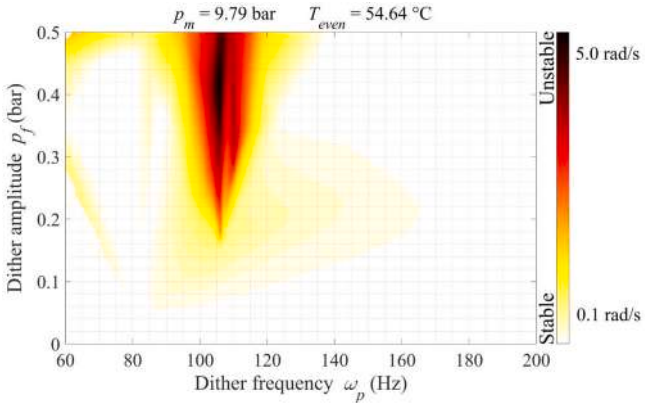

Fig. 10. Experimental stability chart.

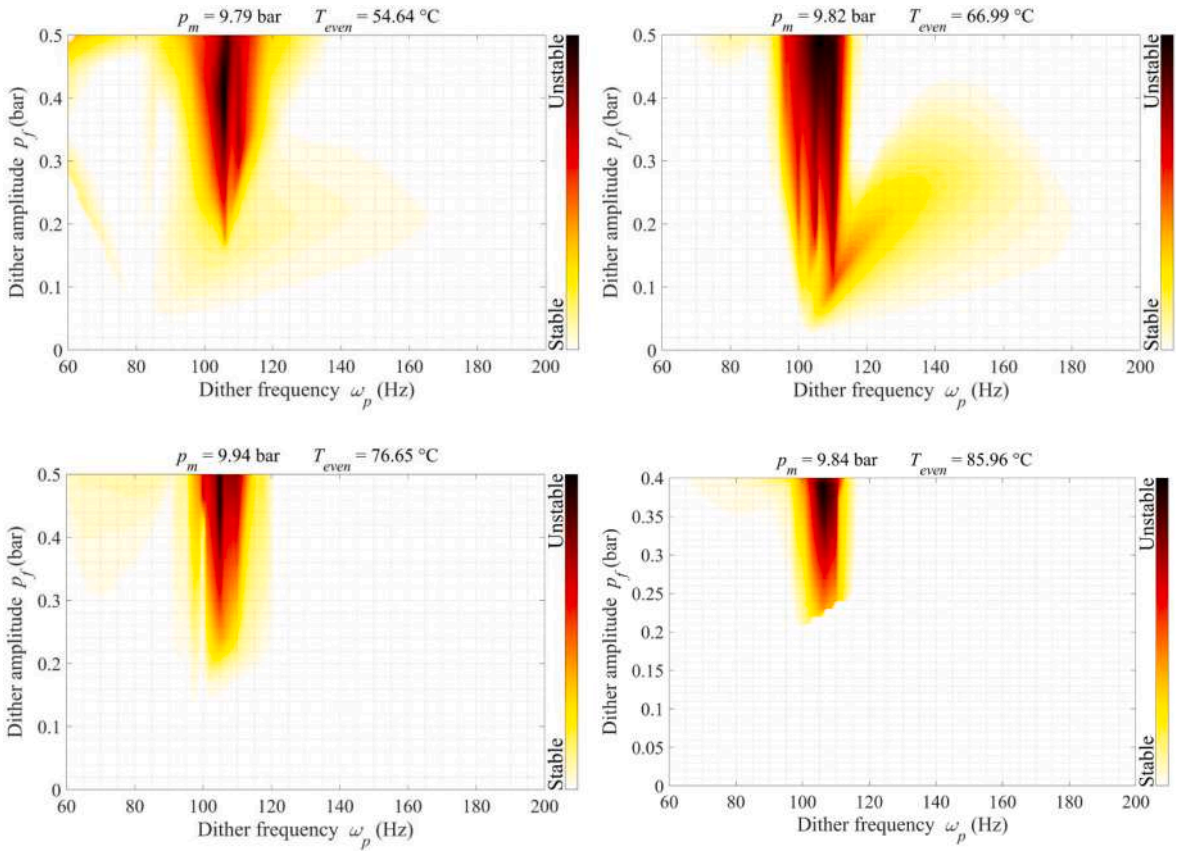

Fig. 11. Experimental stability charts, at different values of oil temperatures.

an external resonance, depending on the transmission characteristics only.

In addition, instability due to a negative gradient of the friction coefficient can be excluded as well for two reasons:

- the experimental data available on the friction surfaces show a positive gradient of the friction coefficient (Fig. 9);
- if the gradient of the friction coefficient had been negative, the system would have been unstable in all the operating conditions below certain damping values (for more details see Fig. 19 in paragraph 4.3).

In conclusion, the features of the observed vibration led to the hypothesis of parametric excitation due to dither in the actuation pressure.

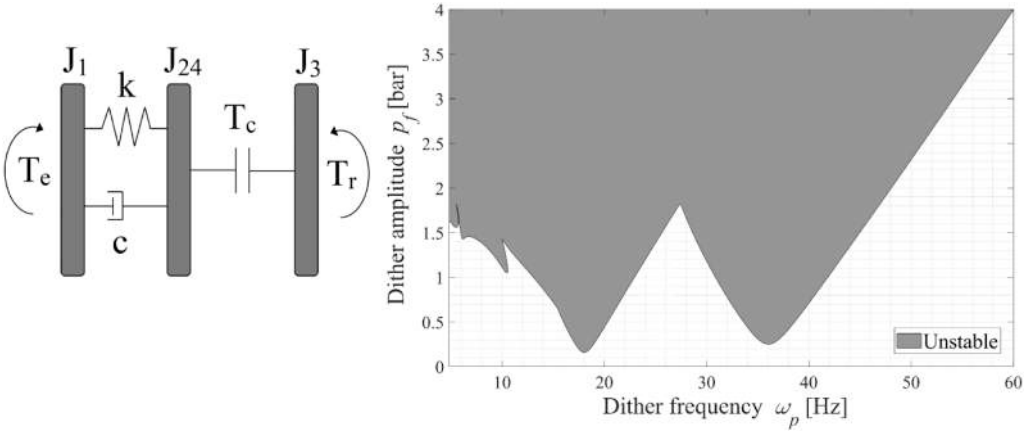

Fig. 12. Schematic of the essential 3 dofs model of the transmission, and its stability map.

3.2. Experimentally estimated stability charts

The time histories recorded in terms of angular speed upstream of the EVEN clutch were transformed into the frequency domain and collected in diagrams drawn as functions of the two excitation parameters, i.e., frequency (ω_p) and amplitude (p_f) of dither, according to the following steps:

- a time history (angular speed) was acquired for each operating condition given by a (ω_p, p_f) pair;
- each time history was Fourier transformed into the frequency domain, identifying its peak amplitude;
- the identified peak amplitudes were reported on a (ω_p, p_f) cartesian contour plot.

This procedure was repeated at several different values of oil temperature, and at different values of engine angular speed.

The contour plots obtained according to this procedure, as the one displayed in Fig. 10, discriminate the regions of a (ω_p, p_f) cartesian diagram by comparing the oscillation amplitudes arising during clutch engagement. From this point of view, therefore, they potentially represent experimentally estimated stability charts. Whether these charts can truly be interpreted as stability maps or not, it should be assessed relying on the analysis of appropriate models, as discussed in the following (see Section 4).

The experimental stability chart displayed in Fig. 10 shows a tongue-shaped region in which judder clearly occurs, featuring a lower tip at about 105 Hz (the dark area). It can be noted that such region closely resembles a so-called Arnold instability tongue, a typical feature of stability maps drawn for parametrically excited systems [28]. This observation also contributes to identify parametric excitation as the source of this particular kind of judder. In all operating conditions contained in the experimental tongue-shaped region, the period of the system response is equal to that of the parametric excitation, i.e., the dither period: this may be interpreted as a single-period Arnold tongue on a stability map.

Diagrams of the same kind of that displayed in Fig. 10 were then obtained by varying the temperature T_{even} of the oil measured near the actuated clutch (EVEN). Four temperature ranges were investigated (covering the operating range of the actual gearbox): 55–60 °C, 65–70 °C, 75–80 °C and 85–90 °C. Temperature has been found to significantly affect the length of the unstable tongue-shaped region. In particular, the worst conditions for stability were found in the temperature range between 65 °C and 70 °C. By increasing or decreasing the temperature with respect to those values, the unstable tongue shortens slightly, and the system stabilizes, as shown in Fig. 11.

During the tests, the temperature $T_{gearbox}$ of the gearbox oil was kept as constant as possible. To ensure these temperature conditions, the execution of each test was started only after the time interval necessary to dissipate the heat generated during the previous engagement and to return to the nominal conditions. By decreasing $T_{gearbox}$, it was observed that the unstable tongue shortens slightly, and the system stabilizes. This may be due to the fact that, as the temperature decreases, the increase in oil viscosity dampens the system.

The charts displayed in Figs. 10 and 11 were obtained at an engine angular speed of 1000 rpm. Tests carried out at 1500 rpm showed a significant contraction of the unstable region (greater than 100%), although its position on the frequency axis remained unchanged. This preliminary result suggests that increasing the input angular speed has a stabilizing effect, which is of great practical importance.

4. Analysis of the experimental results through a minimal model

4.1. Transmission model

The transmission under analysis actually represents a mechanical system with a high level of complexity. From experimental data,

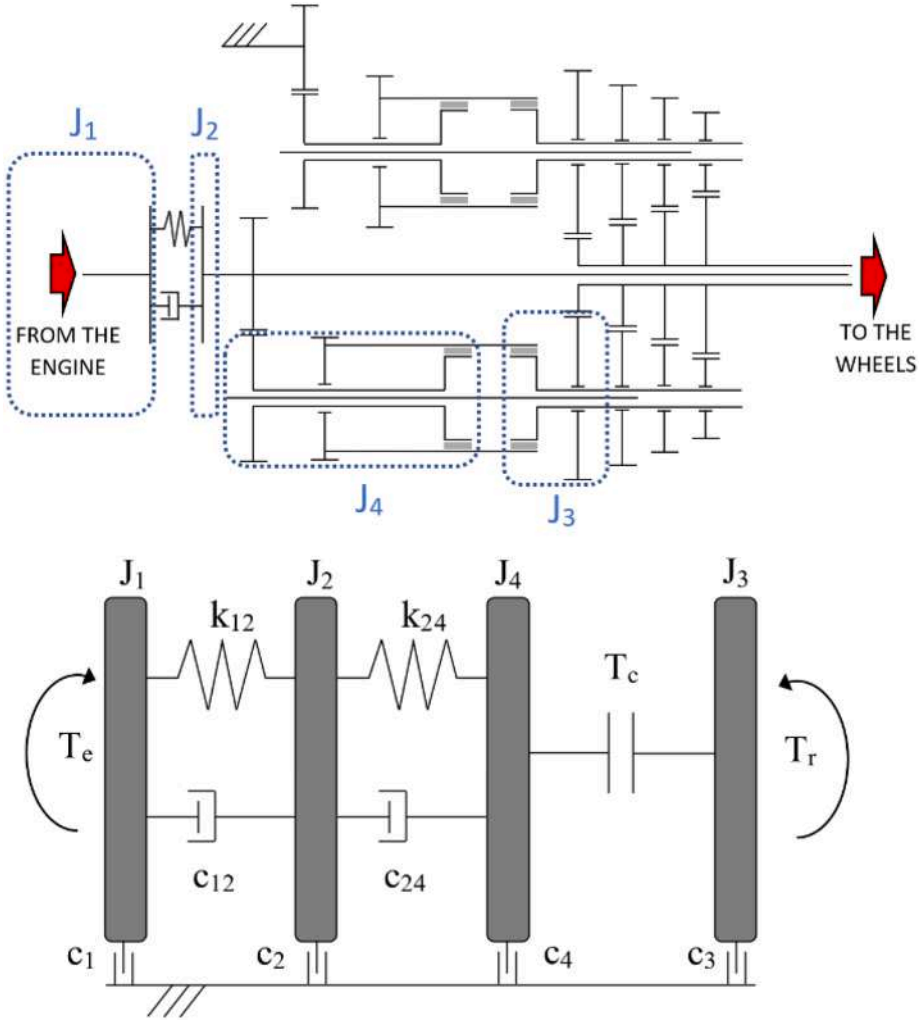

Fig. 13. Schematic of the minimal 4 dofs model of the transmission.

however, a dominant feature strongly emerges (among traces of other possible secondary effects), characterizing the anomalous vibration affecting clutch engagement. In fact, this type of judder primarily manifests itself in a form which is typical of a single-period parametric resonance, in this case excited by dither signal. The oscillations detected on the angular velocity make this fact evident, even if the acquisitions refer to transients (clutch engagements).

Consequently, the first idea for explaining and reproducing such experimentally found behaviour (at least in its dominant feature) was looking for a model as simple as possible, characterized by a reduced number of governing parameters. This choice can also be justified by considering the uncertainties in the estimation of several of the transmission parameters (e.g., friction and damping coefficients, meshing stiffnesses, …), and thus observing that larger models would be affected by the uncertainties related to a larger number of governing parameters, making the analysis more difficult than necessary.

As a first attempt, a minimal 3 dofs model of the transmission was proposed by the authors in a previous work [26] to prove that clutch judder can occur under conditions not contemplated by the current scientific literature. A schematic of this model is shown in Fig. 12, where '1′ represents the body on the engine side (with moment of inertia J_1), '3′ the body on the gearbox side (with moment of inertia J_3) and '2-4′ the body including the clutch damper as well as all the elements placed between the clutch damper and the FWD-EVEN clutch pack (with moment of inertia J_{24}), restrained to '1′ by a torsional spring (k) and a torsional damper (c). In the model, the engine torque is T_e, while the transmitted torque by the clutch is T_c and the resistant torque is T_r.

Specifically, it was shown that the presence of a small fluctuating component in the actuation pressure signal can generate instability due to parametric excitation. This 3 dofs model, however, is not able to fit the experimental data collected in Figs. 10 and 11.

The stability map drawn for the 3 dofs model (adopting the parameter values reported in Appendix) shows two main unstable, tongue-shaped, regions: one of the single-period type (in which the system oscillates with a period equal to that of the parametric excitation) and the other of the double-period type (in which the system oscillates with a double period with respect to the parametric excitation). The single-period region is located at a lower frequency, and it is identified by the only non-zero frequency of vibration of

this model, which refers to the eigenmode characterized by relative oscillations of body '2-4' (essentially, the clutch damper) [26].

Considering that the experimentally found unstable region is located around 105 Hz and that the frequency of vibration of the damper actually is close to 20 Hz, it is evident that this 3 dofs minimal model is unable to quantitatively predict the phenomenon under investigation. Hence it is necessary to increase the complexity of the model.

It was then found that an excellent compromise between accuracy and complexity is given by a specific 4 dofs model (Fig. 13), in which:

- all the components placed between the clutch damper (J_2) and the FWD-EVEN clutch pack have been reduced into a single rotating mass (J_4) and a single torsional stiffness (k_{24}),
- all the components downstream of the FWD-EVEN clutch pack have been reduced into a single rotating mass (J_3).

The equations of motion of the 4 dofs minimal model shown in Fig. 13 read:

$$\boldsymbol{M}\ddot{\boldsymbol{\theta}}(t)+\boldsymbol{C}(t)\dot{\boldsymbol{\theta}}(t)+\boldsymbol{K}\boldsymbol{\theta}(t)=\boldsymbol{g}(t) \tag{1}$$

with:

$$\begin{gathered}\boldsymbol{M}=\begin{bmatrix}J_1&0&0&0\\0&J_2&0&0\\0&0&J_4&0\\0&0&0&J_3\end{bmatrix},\quad \boldsymbol{C}(t)=\begin{bmatrix}c_1+c_{12}&-c_{12}&0&0\\-c_{12}&c_2+c_{12}+c_{24}&-c_{24}&0\\0&-c_{24}&c_4+c_{24}+\mu_g f(t)&-\mu_g f(t)\\0&0&-\mu_g f(t)&c_3+\mu_g f(t)\end{bmatrix}\\ \boldsymbol{K}=\begin{bmatrix}k_{12}&-k_{12}&0&0\\-k_{12}&k_{12}+k_{24}&-k_{24}&0\\0&-k_{24}&k_{24}&0\\0&0&0&0\end{bmatrix},\quad \boldsymbol{\theta}(t)=\begin{bmatrix}\theta_1(t)\\\theta_2(t)\\\theta_4(t)\\\theta_3(t)\end{bmatrix},\quad \boldsymbol{g}(t)=\begin{bmatrix}T_e\\0\\-\mu_0 f(t)\\\mu_0 f(t)-T_r\end{bmatrix}\end{gathered} \tag{2}$$

and:

$$f(t)=N_c R_m S p(t),\quad T_c=\mu(t)N_c R_m S\ p(t) \tag{3}$$

where θ_i is the angular displacement of the rotating element i with inertia J_i and external viscous damping coefficient c_i, c_{ij} and k_{ij} are relative torsional damping and stiffness coefficients between elements i and j, N_c is the number of pairs of clutch plates, R_m is the mean radius of the clutch friction surfaces, $p(t)$ is the actuation pressure, S is the area of action of $p(t)$, T_c is the friction torque and μ is the friction coefficient. The actuation pressure $p(t)$ is composed by a constant (p_m) and an oscillating component (p_f) with angular frequency ω_p (dither):

$$p(t)=p_m+p_f\cos(\omega_p t) \tag{4}$$

As a first approximation, the friction coefficient is considered linearly dependent on the relative speed of the clutch plates, according to:

$$\mu(t)=\mu_0+\mu_g(\dot{\theta}_4-\dot{\theta}_3) \tag{5}$$

Eq. (1) consists of a non-homogeneous system of second order differential equations with periodic coefficients. The parametric excitation affects the damping matrix; therefore, Eq. (1) does not represent a system of Mathieu equations. From Eq. (2) can also be noted the presence of a non-homogeneous term, oscillating with $f(t)$, i.e., with the parametric excitation. By assigning suitable state variables, the system in Eq. (1) can be expressed in the following state-space form:

$$\dot{\boldsymbol{x}}(t)=\begin{bmatrix}\boldsymbol{0}_{4\times4}&\boldsymbol{I}_4\\-\boldsymbol{M}^{-1}\boldsymbol{K}&-\boldsymbol{M}^{-1}\boldsymbol{C}(t)\end{bmatrix}\boldsymbol{x}(t)+\begin{bmatrix}\boldsymbol{0}_{4\times1}\\-\boldsymbol{M}^{-1}\boldsymbol{g}(t)\end{bmatrix},\quad \begin{bmatrix}x_1=\theta_1,\ x_2=\theta_2,\ x_3=\theta_4,\ x_4=\theta_3\\x_5=\dot{\theta}_1,\ x_6=\dot{\theta}_2,\ x_7=\dot{\theta}_4,\ x_8=\dot{\theta}_3\end{bmatrix} \tag{6}$$

Floquet theory can be used to study the stability of differential equations with T-periodic coefficients, but it applies to homogeneous systems [28], in the form:

$$\dot{\boldsymbol{x}}(t)=\boldsymbol{A}(t)\boldsymbol{x}(t),\quad \boldsymbol{A}(t)=\boldsymbol{A}(t+\mathrm{T}) \tag{7}$$

The system in Eq. (6) has a non-homogeneous term including both constant and periodic coefficients. For this stability analysis the constant terms can be neglected. On the other hand, the effects on stability of the non-homogeneous periodic terms are unknown a priori. Therefore, to include non-homogeneous periodic terms in the analysis, two additional state-variables are introduced [29]:

$$x_9(t)=\cos(\omega_p t),\quad x_{10}(t)=\dot{x}_9(t)=-\omega_p\sin(\omega_p t) \tag{8}$$

With the addition of two differential equations, the system in Eq. (6) can be represented in the following homogeneous form:

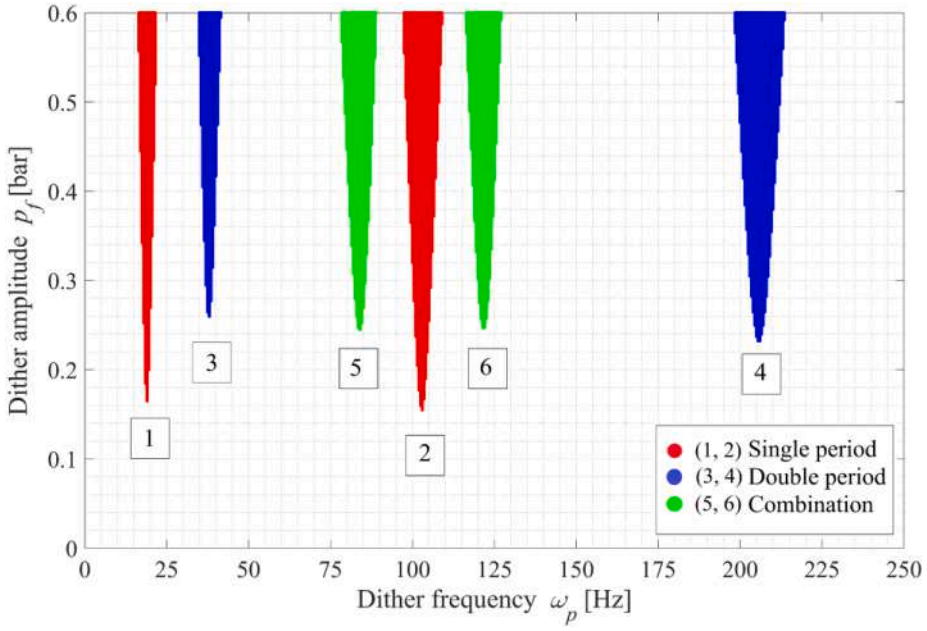

Fig. 14. Stability map obtained with the parameters of the real transmission, as reported in Appendix.

$$\dot{\boldsymbol{x}}(t) = \begin{bmatrix} \mathbf{0}_{4\times4} & \boldsymbol{I}_4 & \mathbf{0}_{4\times1} & \mathbf{0}_{4\times1} \\ -\boldsymbol{M}^{-1}\boldsymbol{K} & -\boldsymbol{M}^{-1}\boldsymbol{C}(t) & \boldsymbol{D} & \mathbf{0}_{4\times1} \\ \mathbf{0}_{1\times4} & \mathbf{0}_{1\times4} & 0 & 1 \\ \mathbf{0}_{1\times4} & \mathbf{0}_{1\times4} & -\omega_p^2 & 0 \end{bmatrix} \boldsymbol{x}(t), \quad \boldsymbol{D} = \begin{bmatrix} 0 \\ 0 \\ -(\mu_0 N_c R_m S p_f)/J_4 \\ (\mu_0 N_c R_m S p_f)/J_3 \end{bmatrix} \tag{9}$$

which can be studied applying Floquet analysis [29].

According to the Floquet-Lyapunov theorem, given a system of n differential equations in the form:

$$\dot{\boldsymbol{x}}(t) = \boldsymbol{A}(t)\boldsymbol{x}(t), \quad \boldsymbol{A}(t) = \boldsymbol{A}(t+T) \tag{10}$$

its *matrizant*, or *principal fundamental matrix*, is expressed by:

$$\boldsymbol{X}(t) = \boldsymbol{F}(t)\, e^{\boldsymbol{B}\ t} \tag{11}$$

where $\mathbf{B}$ is a constant $n \times n$ matrix and $\mathbf{F}(t)$ is a continuous T-periodic $n \times n$ matrix, non-singular for all t and such that $\mathbf{F}(0) = \mathbf{I}_n$ (identity matrix of dimension n). Therefore, the asymptotic behaviour of the system entirely depends on the matrix $\mathbf{B}$, and its stability can be assessed by considering the eigenvalues of $\mathbf{B}$, called *characteristic exponents* or *Floquet exponents*.

Moreover, let $\mathbf{X}(T)$ be the matrizant of the system in Eq. (10) evaluated at $t = T$, and let $\lambda_1, \ldots, \lambda_n$ be its eigenvalues. Then, $\mathbf{X}(T)$ is called *monodromy matrix* or *Floquet Transition Matrix* (FTM) and λ_i is called *Floquet multiplier*. The *i-th* Floquet multiplier and the *i-th* characteristic exponent α_i are linked by:

$$\lambda_i = e^{\alpha_i T} \tag{12}$$

Unlike Floquet multipliers, each characteristic exponent is not unique, since an infinite number of other characteristic exponents can be obtained from the same α_i:

$$\lambda_i = e^{\left(\alpha_i + \mathrm{i}\frac{2\pi m}{T}\right)T}, \quad m \in \mathbb{N} \tag{13}$$

where i denotes the imaginary unit.

In summary, the stability of a parametrically excited system can be assessed by evaluating either the eigenvalues of the monodromy matrix (Floquet multipliers) or the eigenvalues of matrix $\mathbf{B}$ (characteristic exponents).

Note that the presence of the non-homogeneous term in Eq. (1) does not modify the stability threshold of the problem, however it can determine resonance conditions within the stable regions.

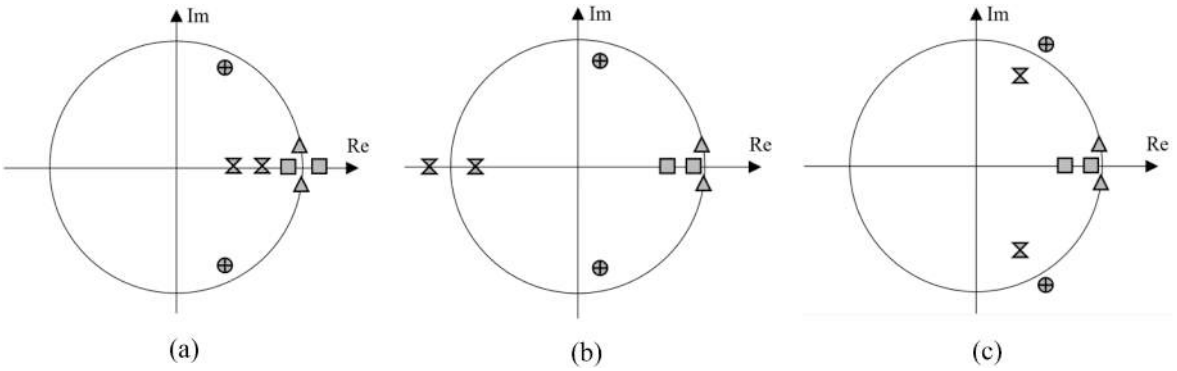

Fig. 15. Position of the Floquet multipliers on the complex plane (for clarity the graphs are not to scale). (a) Single-period instability; (b) double-period instability; (c) combination-type instability.

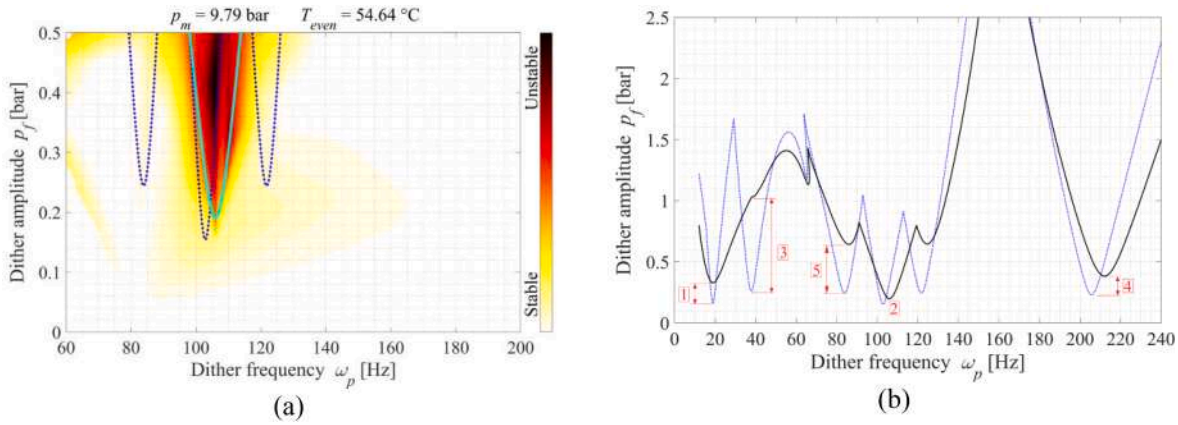

Fig. 16. The dotted line is due to stability analysis of the 4 dofs model with the parameters in Appendix, while the solid line is obtained by varying some parameters of difficult estimation (c_{12}, μ_p and k_{24}).

4.2. Fitting experimental data

The values adopted for the parameters in the 4 dofs model, reported in Appendix B, are those obtained from the actual transmission and test bench. The only parameters that could not be estimated are the damping coefficients, for which first attempt values, but not actual values were used. The computation of the Floquet multipliers [28] of the system given in Eq. (9) yields the stability map displayed in Fig. 14.

Considering the homogeneous system without damping matrix:

$$\boldsymbol{M}\ddot{\theta}(t) + \boldsymbol{K}\theta(t) = \boldsymbol{0} \tag{14}$$

it is possible to determine the only two non-zero eigenfrequencies of the system:

$$(\omega_{1,2})^2 = \frac{J_4 k_{12}(J_1 + J_2) + J_1 k_{24}(J_2 + J_4) \pm \sqrt{\Delta}}{2 J_1 J_2 J_4}$$
$$\Delta = [J_4 k_{12}(J_1 + J_2)]^2 + [J_1 k_{24}(J_2 + J_4)]^2 + 2 J_1 J_4 k_{12} k_{24}[J_4(J_1 - J_2) - J_2(J_1 + J_2)] \tag{15}$$

The remaining two eigenfrequencies of the system are zero as they are associated with rigid body motions.

The instability regions associated to the tongues 1 and 2 displayed in Fig. 14 have their tips positioned on the two non-zero eigenfrequencies of the system (18.9 Hz and 102.9 Hz from Eq. (15)) and give rise to a single-period instability, therefore the period of the angular response is equal to the period of the parametric excitation (dither). In this case, the Floquet multiplier that makes the system unstable leaves the unit circle of the Argand plane on the real positive semi-axis, as shown in Fig. 15a.

The instability regions associated to the tongues 3 and 4 are of double-period type, and this is due to a Floquet multiplier that comes out of the unit circle on the real negative semi-axis, as shown in Fig. 15b.

Finally, the instability regions associated to the tongues 5 and 6 are generated by pairs of complex conjugate multipliers crossing the unit circle in the complex plane, as shown in Fig. 15c, and they are called combination instability regions. If the period of the

solution corresponding to such critical multipliers is not an integer multiple of the dither period, the system response is non-periodic [28,30,31,32]. In Fig. 14, the single-period tongue 2 and the combination tongues 5 and 6 form a sort of large unstable tricuspid tongue.

The morphology of the stability map obtained for the 4 dofs model can be explained relying on the analysis of the minimal 3 dofs model presented by the authors in a previous work [26]. In fact, as expected, the fourth degree of freedom adds a single-period and the corresponding double-period tongue. Furthermore, the 4 dofs model shows a different feature: the two unstable regions 5 and 6 in Fig. 14. These regions arise from the fact that there is more than one pair of complex conjugate multipliers able to cross the unit circle in the complex plane.

The comparison between the experimental chart displayed in Fig. 10, and the stability map obtained from the 4 dofs model in Fig. 14 shows a good overlap already with first attempt parameters, as can be seen in Fig. 16a. The unstable single-period region detected on the test bench is predicted with good accuracy by the minimal model. The dotted line is the first attempt boundary, obtained using the damping coefficient for the clutch damper as reported in Appendix (selected on purpose as a very low first attempt value).

To compare the damping levels in the clutch damper, it is useful to consider damping factors, rather than damping coefficients. By considering the clutch damper as an isolated single-degree-of-freedom system, its damping factor can be defined as:

$$\zeta_{12}(\%) = 100\frac{c_{12}}{2\sqrt{k_{12}J_2}} \tag{16}$$

yielding 0.9% using the first attempt damping coefficient reported in Appendix.

The solid line in Fig. 16 was obtained by modifying some parameters that are difficult to estimate. In the specific case, the damping factor was increased from 0.9% (0.5 Nms/rad) to 17% (10 Nms/rad), the gradient of the friction coefficient from 0.017 to 0.022 and the equivalent stiffness k_{24} was increased by about 6%. The dotted line in Fig. 16 is composed by a central single-period tongue and two symmetrical unstable combination regions: the latter were not detected during the tests, which may be due to higher damping values of the actual clutch damper. In fact, as the damping factor associated to the clutch damper is increased (solid line), the two combination tongues shorten and disappear from the operating range of the dither.

The influence on the stability threshold of the damping factor of the clutch damper may also explain the fact that the experimental tests did not show other unstable tongues in the small range of dither amplitudes. This is highlighted in Fig. 16b which shows a clear difference in the contraction of the various instability tongues. In particular:

- tongue 3 (double-period type) disappears completely and symmetrical tongues 5 (combination type) also contract until they almost vanish;
- the single-period tongue 1 and the double-period tongue 4 undergo a very marked contraction that could take them out of the operating range of dither;
- the single-period tongue 2, that is the one observed experimentally, remains almost unchanged.

In addition to assuming a very low damping factor for the clutch damper (as in Appendix), the presence on the theoretical map of unstable tongues not detected experimentally can also have other explanations.

First, the transients of the engagement may not last long enough to appreciate the instability. Indeed, unstable solutions can have different growth rates, depending on their position on the stability map. Secondly, the adopted model does not consider several aspects of the complexity of the real transmission, such as nonlinear effects and asymmetries, able to produce relevant modifications in the stability thresholds (among them, also 'merging' effects between adjacent instability tongues [32,33]).

The experimental stability map was obtained in the operating range of dither (60 – 200 Hz), and not extended to lower frequency values, as valve control deteriorates by decreasing too much the dither frequency. Although it was not possible to verify the presence of the low frequency single-period region (tongue 1 in Fig. 14), it is interesting to note that some tests prior to the experimental campaign of this study (Introduction, Fig. 1) clearly show an anomalous vibration around 20 Hz. This evidence further contributes to highlighting the validity of the developed model.

In summary, the proposed model is able to identify the principal single-period unstable region with very good accuracy with respect to experimental data. Therefore, it can be adopted as a predictive tool to design the transmission and set its operating parameters in order to avoid, already in the design phase, the possibility of having this kind of clutch judder. To this purpose, the predicted unstable region may be identified as the broadest region obtained by considering all the variation ranges of parameters due to uncertainties in their estimation.

4.3. Sensitivity analysis of the 4 dofs model

A sensitivity analysis of the model was carried out to observe the effects of each of its governing parameters on the stability maps. Each of the following figures compares the nominal stability boundary (obtained with the parameters reported in Appendix) with the two stability boundaries obtained by doubling and halving the nominal value of each parameter.

The most evident effect of torsional stiffnesses and moments of inertia is the translation of Arnold's tongues on the frequency axis (Fig. 17). Together with this effect, due to the variation of the eigenfrequencies of the system, there is also a shift of the stability boundary on the y axis, appreciable at high amplitudes of parametric excitation.

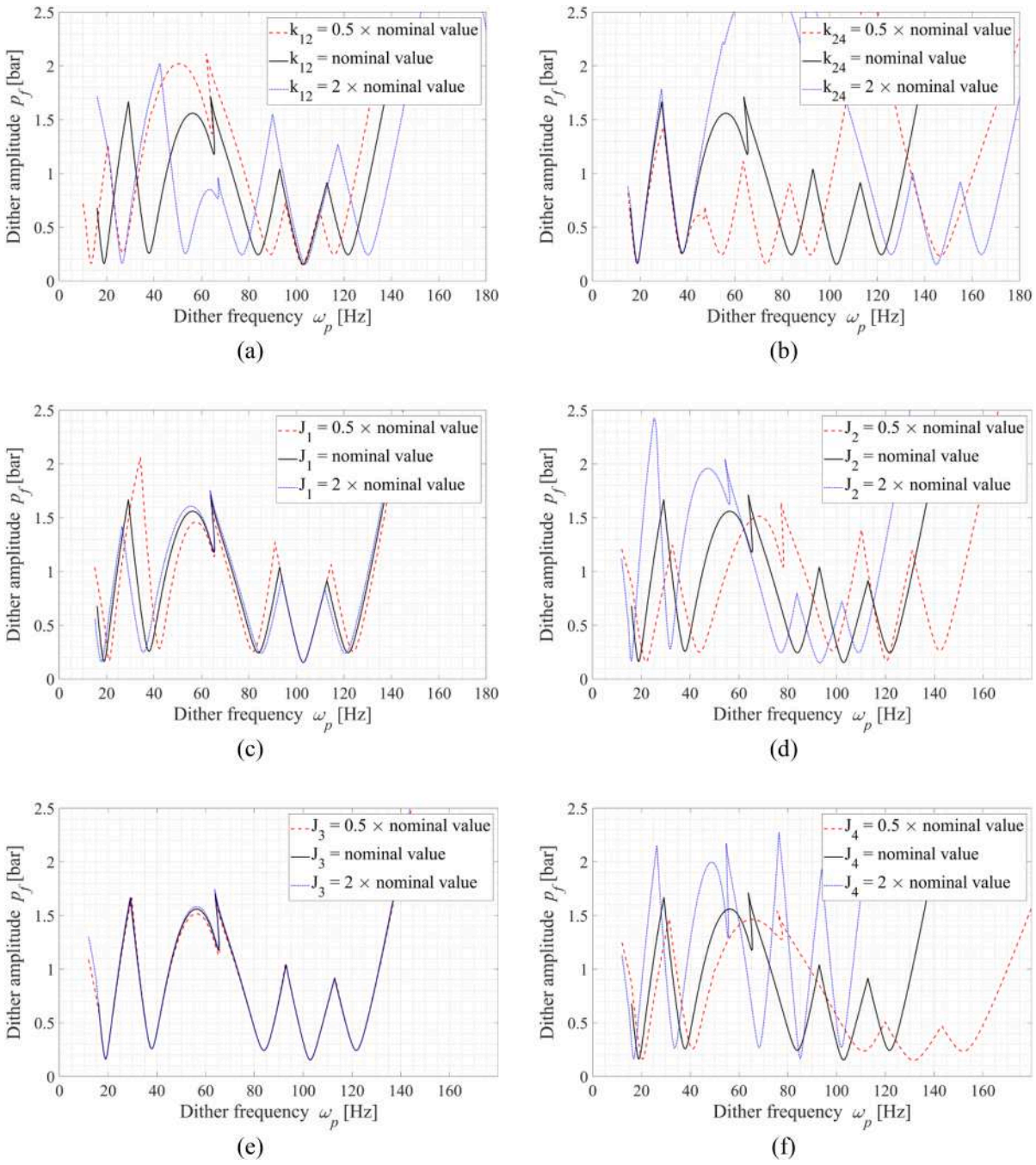

Fig. 17. Effects on the stability boundary of: (a) k_{12}; (b) k_{24}; (c) J_1; (d) J_2; (e) J_3; (f) J_4.

Parameter k_{12} is the torsional stiffness of the clutch damper and especially affects low-frequency unstable tongues, as shown in Fig. 17a. This result is quite intuitive as the characteristics of the damper mainly modify the frequency of the first eigenmode of the system, as emerges from Eq. (15).

Parameter k_{24} is the equivalent stiffness of the components located between the damper and the clutch. Essentially k_{24} can be approximated with the stiffness of the transmission shaft that connects the clutch damper to the first gear wheel, since the other stiffnesses involved are of some order of magnitude greater.

Parameter k_{24} mainly modifies the second frequency of vibration of the system, so its effects are evident on the high frequency single-period tongue and cause its translation on the frequency axis (Fig. 17b).

The moments of inertia of rotating bodies have effects similar to those of stiffness, but antithetical. In fact, while the increase in

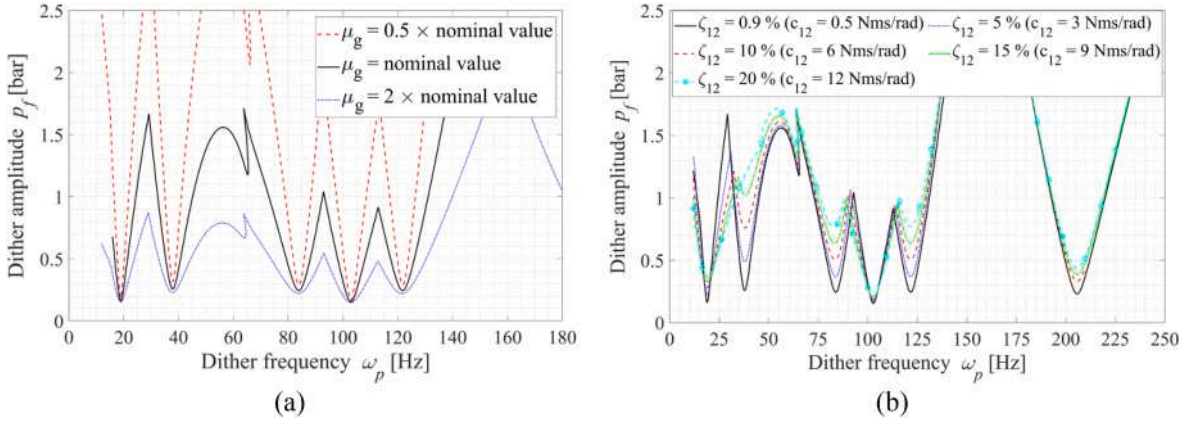

Fig. 18. Effects on the stability boundary of μ_g (a) and c_{12} (b).

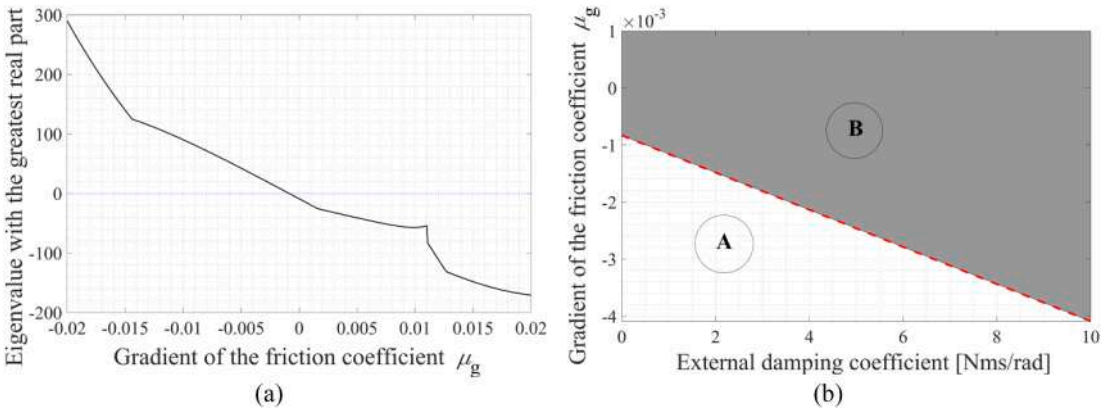

Fig. 19. Non-parametrically excited 4 dofs model. (a) Transition from the stable zone (lower half-plane) to the unstable one (upper half-plane) by reducing the gradient of the friction coefficient. (b) Stability threshold in the $c_i - \mu_g$ plane.

stiffness moves the unstable regions to higher frequencies, the increase in the moments of inertia moves them to lower frequencies.

Parameters J_2 and J_4 have the greatest effects on the stability map (Fig. 17d and f), while J_1 has little influence (Fig. 17c) and J_3 has negligible effects (Fig. 17e). In particular, the single-period tongue experimentally detected with its tip close to 100 Hz is not affected at all by the moment of inertia J_1 upstream of the clutch damper, nor by the moment of inertia J_3 downstream of the clutches.

In the equations of motion of the 4 dofs model, the coefficient of friction between the clutch plates appears only between the non-homogeneous terms. In particular, for the specific case, stability analysis showed that the non-homogeneous terms do not modify the stability threshold, therefore from this point of view the model is insensitive to variations in the friction coefficient. On the other hand, the effect of the gradient of the friction coefficient on the stability maps is of practical interest as it multiplies some time-varying coefficients of the damping matrix.

As the gradient of the friction coefficient decreases, the instability tongues progressively taper off (Fig. 18a) until they reach a threshold of mere stability. Parallel to this effect, a shortening of the unstable tongues is also observed.

Considering the system described in Eqs. (1) to (5) without parametric excitation ($p_f = 0$), and varying the gradient of the friction coefficient, it is possible to verify its stability through the values of the real parts of its eigenvalues. Fig. 19a shows the trend of the value of the greatest real part among the eigenvalues as a function of the gradient of the coefficient of friction. The points of the curve above the x-axis correspond to conditions of instability. So, the point of intersection of the curve with the x-axis represents the stability threshold, in which conditions the solution is merely (or simply) stable. Once this threshold is exceeded, the solution becomes unstable in all conditions, regardless of whether the system is parametrically excited or not, as the cause of the instability is no longer parametric excitation.

The threshold of mere stability is affected by external damping coefficients c_i. By increasing the external damping, the threshold shifts towards negative values of the gradient of the coefficient of friction. A stability map in the $c_i - \mu_g$ plane is displayed in Fig. 19b, where in region A there is instability in all conditions, while in region B the solutions of the non-parametrically excited system are stable, and instability can occur due to parametric excitation.

The analyzed 4 dofs model features both external and internal damping elements, to consider the damping of the components connecting the rotating bodies each other, as well as the damping exerted by the lubricating oil and by the bearings.

For high excitation amplitudes and in the case of internal damping, it has been shown in [26] that an increase in damping can have a destabilizing effect as the unstable region widens, albeit slightly. Despite this, in general, the increase in the damping coefficients causes a contraction of the tips of Arnold's tongues. Therefore, in the operating range of dither, i.e., for low values of the parametric excitation amplitude, the effect of internal damping is stabilizing.

Here it can also be noted that in parametrically excited systems with multiple degrees of freedom, the stabilizing effect of damping is more effective on higher order modes (or more precisely, on those Floquet multipliers related to higher frequency modes of the non-parametrically excited system). Therefore, the stability thresholds in this kind of problems are usually determined by the contribution of the lower modes only (since the effect of the higher spectrum of natural frequencies is cleared by damping [32,34]). This is particularly important in the case under analysis, and for the effectiveness of a minimal model like the one described in Section 4.1.

In the case under study, it is relevant to observe the particular effect of the damping coefficient of the clutch damper (c_{12}), as it affects double-period and combination resonances tongues much more than single-period tongues, as already noticed in Section 4.2. This could help to explain why some unstable areas in the model were not detected in the tests. In fact, the torsional damping coefficient of a clutch damper can have a very wide range of variability (from about 10 to over 1000 Nms rad^{-1}, according to data reported in the literature [35,36]), so a value of the damping coefficient c_{12} higher than that reported in Appendix (i.e. a damping factor greater than 20%) is more realistic and could bring non-single-period tongues above the operating range of dither.

By plotting the stability maps with higher c_{12} values (Fig. 18b), the two combination tongues (near 80 and 120 Hz) and the double-period tongue (near 40 Hz) contract until they disappear. The single-period tongue near 20 Hz and the double-period one near 210 Hz significantly contract and, even if they do not disappear, they can still come out of the dither operating area leaving only the unstable region around 105 Hz, which remains almost unchanged. Recalling Eq. (16), the model shows that with ζ_{12} greater than 17% the unstable regions 5 and 6 displayed in Fig. 14 are found at fluctuating pressure values greater than 0.7 bar, therefore reasonably outside the dither operating range.

On the other hand, the effects of the internal damping coefficient c_{24} and the external damping coefficients c_i are not noticeable with relatively small variations of the values reported in Appendix. For much higher values, as already mentioned, they are able to produce widespread contractions of unstable regions.

5. Conclusions

This work shows that clutch judder can also be caused by a parametric excitation due to actuation pressure, thus it can occur in a wider spectrum of conditions than reported in the scientific literature.

This kind of judder was investigated by processing experimental data (time histories) acquired on a specifically designed test bench. A minimal model with 4 degrees of freedom was then proposed, able to fit the experimental data, to explain the onset of the parametrically excited vibration, and to identify which parameters have a major role in controlling the phenomenon (dither frequency and amplitude).

Based on the sensitivity analysis carried out on the model, it was possible to identify, in order of priority, the transmission parameters to be modified to bring the unstable region out of the dither operating range and thereby stabilize the system. In particular, the equivalent stiffness and moments of inertia of the components between the damper and the clutches are the parameters that were found to have the greatest influence on the unstable region experimentally detected.

Although not experimentally verified, the damping factor of the clutch damper is expected to play a key role: below a certain value, it could generate other areas of parametric instability. Furthermore, the external damping coefficients, despite their non-striking effect on the stability maps, move the threshold of the gradient of the friction coefficient. Below this threshold the system becomes unstable in all conditions, even if not parametrically excited.

In summary, the proposed analysis provides tools that allow to predict instability conditions and to avoid them already in the design phase.

Declaration of Competing Interest

The authors declare that they have no known competing financial interests or personal relationships that could have appeared to influence the work reported in this paper.

Data availability

The data that has been used is confidential.

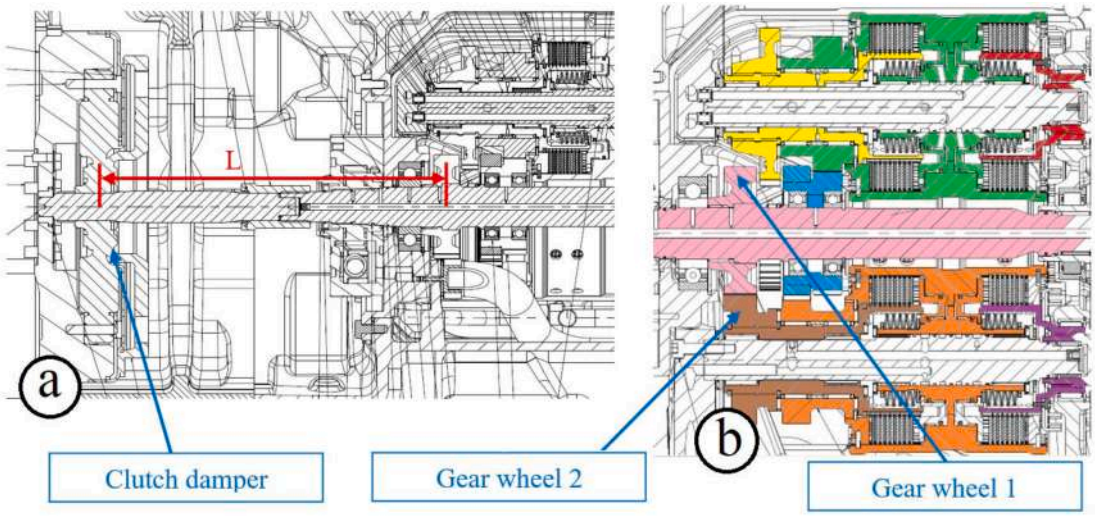

Fig. 20. Transmission components contributing to the equivalent stiffness k_{24}.

Appendix A

Values adopted for the parameters

3 DOFS MODEL

Model parameter		Model parameter		Model parameter	
J_1	1.12 kg m^2	k	3451 N m rad^{-1}	μ_g	0.017
J_{24}	0.353 kg m^2	c	0.5 N m s rad^{-1}	μ_0	0.09
J_3	4.07 kg m^2				

4 DOFS MODEL

Model parameter		Model parameter		Model parameter	
J_1	1.12 kg m^2	k_{12}	3856 N m rad^{-1}	μ_0	0.09
J_2	0.231 kg m^2	k_{24}	32885 N m rad^{-1}	μ_g	0.017
J_3	4.07 kg m^2	c_{12}	0.5 N m s rad^{-1}	c_i	0.1 N m s rad^{-1}
J_4	0.122 kg m^2	c_{24}	0.1 N m s rad^{-1}		

The parameter values of the models have been obtained from the technical documentation provided by CNH Industrial. The moments of inertia of the transmission components have been calculated by the CAD software: in the model they have been merged into equivalent moments of inertia taking into account the reduction ratios of the gears. The stiffness coefficients have been calculated from the dimensional drawings and technical specifications. In particular, the stiffness coefficient k_{12} is a technical specification of the torsional damper, while k_{24} is an equivalent stiffness coefficient resulting from two stiffnesses in series: the torsional stiffness of the shaft L in Fig. 20a and the mesh stiffness between the gear wheels highlighted in Fig. 20b. The damping coefficients have been assumed, while the friction coefficient and its gradient have been estimated from the experimental graphs of Fig. 9.

References

[1] D. Centea, H. Rahnejat, M.T. Menday, The influence of the interface coefficient of friction upon the propensity to judder in automotive clutches, Proc. Inst. Mech. Eng. D: J. Automob. Eng. 213 (5) (1999) 245–258, https://doi.org/10.1243/0954407991526847.
[2] I. Minas, N. Morris, S. Theodossiades, M. O'Mahony, J. Voveris, On the Effect of Clutch Dynamic Properties on Noise, Vibration and Harshness Phenomena, SAE Int, J. Adv. Curr. Pract. Mobil. 3 (2) (2021) 1059–1067, https://doi.org/10.4271/2020-01-1510.
[3] P. Wickramarachi, R. Singh, G. Bailey, Analysis of Friction-Induced Vibration Leading to 'EEK' Noise in a Dry Friction Clutch, Noise Control Eng. J. 53 (4) (2005) 138–144, https://doi.org/10.3397/1.2839252.
[4] Y. Aktir, J.F. Brunel, P. Dufrenoy, H. Mahé, Modeling Squeal Noise on Dry Automotive Clutch, in: Proc. ISMA 2014 - Int. Conf. Noise Vib. Eng. and USD 2014 - Int. Conf. Uncertain. Struct. Dyn. pp. (2014) 1813–1826.
[5] A. Fidlin, O. Drozdetskaya, B. Waltersberger, On the Minimal Model for the Low Frequency Wobbling Instability of Friction Discs, Eur. J. Mech. A/Solids 30 (5) (2011) 665–672, https://doi.org/10.1016/j.euromechsol.2011.03.009.
[6] T. Gkinis, R. Rahmani, H. Rahnejat, Effect of clutch lining frictional characteristics on take-up judder, in: Proc. Inst. Mech. Eng. K: J. Multi-body Dyn. 231 (3) (2017) 493–503. 10.1177/1464419317708946.

[7] P. Maucher, Clutch Chatter, in: Proc. 4th Int. Symp. Tors. Vib. Drive Train (1990) 109–124.
[8] C. Bostwick, A. Szadkowski, Self-Excited Vibrations during Engagements of Dry Friction Clutches, SAE Tech. Pap. 982846 (1998), https://doi.org/10.4271/982846.
[9] A. Crowther, N. Zhang, D. Liu, J. Jeyakumaran, Analysis and Simulation of Clutch Engagement Judder and Stick-Slip in Automotive Power Train System, in: Proc. Inst. Mech. Eng. Part D: J. Automob. Eng. 218 (12) (2004) 1427–1446. 10.1243/0954407042707731.
[10] S. Iqbal, F. Al-Bender, A.P. Ompusunggu, B. Pluymers, W. Desmet, Modeling and Analysis of Wet Friction Clutch Engagement Dynamics, Mech. Syst. Signal Process. 60 (2015) 420–436, https://doi.org/10.1016/j.ymssp.2014.12.024.
[11] S. Mohire, R. Kapse, V. Tendulkar, Study of Clutch Judder Phenomenon in Manual Transmission Vehicle and Its Analysis Approach, SAE Tech. Pap. 2019-26-0215 (2019). 10.4271/2019-26-0215.
[12] T. Kugimiya, N. Yoshimura, J. Mitsui, Tribology of Automatic Transmission Fluid, Tribol. Lett. 5 (1) (1998) 49–56, https://doi.org/10.1023/A:1019156716891.
[13] J. Zhang, B. Ma, M. Zehn, Study on Clutch Engagement Judder during Launch Process for Dual Clutch Transmissions, Int. J. Veh. Noise Vib. 6 (2–4) (2010) 176–199, https://doi.org/10.1504/IJVNV.2010.036685.
[14] D. Centea, H. Rahnejat, M.T. Menday, Non-Linear Multi-Body Dynamic Analysis for the Study of Clutch Torsional Vibrations (Judder), Appl. Math. Model. 25 (3) (2001) 177–192, https://doi.org/10.1016/S0307-904X(00)00051-2.
[15] L. Li, Z. Lu, X.L. Liu, T. Sun, X. Jing, W. Bin Shangguan, Modeling and analysis of friction clutch at a driveline for suppressing car starting judder, J. Sound Vib. 424 (2018) 335–351, https://doi.org/10.1016/j.jsv.2018.03.011.
[16] T.P. Newcomb, R.T. Spurr, Clutch Judder, in: Proc. XIVth Int. Automob. Tech. Congr. FISITA (1972) 1/16–1/18.
[17] R.P. Jarvis, B. Mills, Vibrations Induced by Dry Friction, Proc. Inst. Mech. Eng. 178 (1) (1963) 847–857, https://doi.org/10.1177/002034836317800112 4.
[18] M. Pandey, R.H. Rand, A.T. Zehnder, Frequency Locking in a Forced Mathieu-van Der Pol-Duffing System, Nonlinear Dyn. 54 (1–2) (2008) 3–12, https://doi.org/10.1007/s11071-007-9238-x.
[19] K. Berglund, P. Marklund, H. Lundh, R. Larsson, Prediction of Driveline Vibrations Caused by Ageing the Limited Slip Coupling, Proc. Inst. Mech. Eng. D: J. Automob. Eng. 230 (12) (2016) 1687–1698, https://doi.org/10.1177/0954407015619505.
[20] J.R. Barber, Thermoelastic instabilities in the sliding of conforming solids, Proc. R. Soc. A 312 (1510) (1969) 381–394, https://doi.org/10.1098/rspa.1969.0165.
[21] Y.B. Yi, J.R. Barber, P. Zagrodzki, Eigenvalue solution of thermoelastic instability problems using Fourier reduction, Proc. R. Soc. A 456 (2003) (2000) 2799–2821, https://doi.org/10.1098/RSPA.2000.0641.
[22] T. Paygude, R. Joshi, Modeling and Analysis of Clutch Engagement Judder in Commercial Vehicle Powertrain Systems. SAE Tech. Pap. 2019-01-0784 (2019). 10.4271/2019-01-0784.
[23] L.K. Yang, H.Y. Li, M. Ahmadian, B. Ma, Analysis of the Influence of Engine Torque Excitation on Clutch Judder, J. Vib. Control 23 (4) (2017) 645–655, https://doi.org/10.1177/1077546315582291.
[24] O. Reinertz, A comparative study on dither signals and their parameterization. In: Proc. 11th Int. Fluid Power Conf. 3/ (2018)/ 270–282.
[25] M. Sivanesan, G. Jayabalaji, Modelling, Analysis and Simulation of Clutch Engagement Judder and Stick-Slip. SAE Int. J. Passeng. Cars - Mech. Syst. 10 (1) (2017) 54–64. 10.4271/2016-01-2355.
[26] M. Tentarelli, S. Cantelli, A. De Felice, S. Sorrentino, Cold Judder in Tractor Drivelines: an Essential Model for Stability Analysis, in A. Orlova and and D. Cole (Eds.): Adv. Dyn. Veh. Road Tracks II - IAVSD 2021 (2022) 736–746, Springer Nature, Switzerland. 10.1007/978-3-031-07305-2_69.
[27] M. Tentarelli, S. Cantelli, S. Sorrentino, A. De Felice, Experimental stability analysis of tractor drivelines affected by cold judder, in: Proc. Int. Conf. Noise Vib. Eng. – ISMA (2022), Leuven, Belgium, September 12-14. https://past.isma-isaac.be/isma2022/proceedings/program/#Self-excited%20vibrations.
[28] V.A. Yakubovich, V.M. Starzhinski, Linear Differential Equations with Periodic Coefficients, John Wiley and Sons, New York, 1975.
[29] S.M. Forghani, T.G. Ritto, Stochastic stability of the non-homogeneous damped Mathieu equation, Nonlinear Dyn. 86 (2016) 1561–1570, https://doi.org/10.1007/s11071-016-2977-9.
[30] A. De Felice, S. Sorrentino. Insights into the gyroscopic behaviour of axially and torsionally loaded rotating shafts, in: Proc. 24th Int. Conf. Sound Vib. (ICSV24). (2017). London, United Kingdom. July 23-27.
[31] A. De Felice, S. Sorrentino. Stability Analysis of Parametrically Excited Gyroscopic Systems, in: Proc. XXIV Conf. Ital. Assoc. Theor. Appl. Mech. – AIMETA XXIV. (2019). 1316–1331. 10.1007/978-3-030-41057-5_106.
[32] A. De Felice. S. Sorrentino. Damping and Gyroscopic Effects on the Stability of Parametrically Excited Continuous Rotor Systems, Nonlinear Dyn. 103 (4). (2021). 3529–3555. 10.1007/s11071-020-06106-3.
[33] A. De Felice, S. Sorrentino, Effects of anisotropic supports on the stability of parametrically excited slender rotors, Nonlinear Dyn. (2022), https://doi.org/10.1007/S11071-022-07487-3.
[34] A. De Felice, S. Sorrentino. The second spectrum in Timoshenko beam theory: a new approach for its identification, in: Proc. 25th Int. Conf. Sound Vib. – ICSV25 8. (2018). 4640–4647. 2018. Hiroshima, Japan. July 8-12.
[35] T. Kodama, Y. Honda. A Study on the Modeling and Dynamic Characteristics of the Viscous Damper Silicone Fluid by Using Vibration Control of Engine Crankshaft System. Int. J. Mech. Eng. and Robot. Res. 7 (3). (2018). 273-278. 10.18178/ijmerr.7.3.273-278.
[36] K. Wakabayashi, Y. Honda, T. Kodama, S. Iwamoto, The Dynamic Characteristics of Torsional Viscous-Friction Dampers on Reciprocating Engine Shaftings, SAE Tech. Pap. 101 (1992) 1734–1754, https://doi.org/10.4271/921726.